Vicente Durán-Toro, Kurosch Rezwan, Solveig I. Bühring,Michael Maas

Arsenic and sulfur nanoparticle synthesismimicking environmental conditions of submarineshallow-water hydrothermal vents

Journal Article	as:	peer-reviewed accepted version (Postprint)
DOI of this document*(secondary publication):		https://doi.org/10.26092/elib/2811
Publication date of this document:		06/03/2024

* for better findability or for reliable citation

Recommended Citation (primary publication/Version of Record) incl. DOI:

Vicente Durán-Toro, Kurosch Rezwan, Solveig I. Bühring, Michael Maas,
Arsenic and sulfur nanoparticle synthesis mimicking environmental conditions of submarine shallow-water hydrothermal vents, Journal of Environmental Sciences, Volume 111, 2022, Pages 301-312,
ISSN 1001-0742,
https://doi.org/10.1016/j.jes.2021.04.011.

Arsenic and sulfur nanoparticle synthesis mimicking environmental conditions of submarine shallow-water hydrothermal vents

Vicente Durán-Toro[1,*], *Kurosch Rezwan*[2,3], *Solveig I. Bühring*[1], *Michael Maas*[2,3,*]

[1] *MARUM – Center for Marine Environmental Sciences, University of Bremen, Bremen 28359, Germany*
[2] *Advanced Ceramics, University of Bremen, Bremen 28359, Germany*
[3] *MAPEX - Center for Materials and Processes, University of Bremen, Bremen 28359, Germany*

Keywords:
Biomineralization
Milos
Hydrothermal vent
Arsenic
Sulfur
Nanoparticles
Ecotoxicology

ABSTRACT

Arsenic and sulfur mineralization is a natural phenomenon occurring in hydrothermal systems where parameters like temperature and organic matter (OM) can influence the mobilization of the toxic metalloid in marine environments. In the present study we analyze the influence of temperature and OM (particularly sulfur-containing additives) on As and S precipitation based on the recent discovery of As-rich nanoparticles in the hydrothermal system near the coast of the Greek island Milos. To this end, we experimentally recreate the formation of amorphous colloidal particles rich in As and S via acidification (pH 3–4) of aqueous precursors at various temperatures. At higher temperatures, we observe the formation of monodisperse particles within the first 24 h of the experiment, generating colloidal particles with diameters close to 160 nm. The S:As ratio and particle size of the synthetized particles closely correlates with values for As_xS_y particles detected in the hydrothermal system off Milos. Furthermore, organic sulfur containing additives (cysteine and glutathione, GSH) are a key factor in the process of nucleation and growth of amorphous colloidal As_xS_y particles and, together with the temperature gradient present in shallow hydrothermal vents, dictate the stabilization of As-bearing nanomaterials in the environment. Based on these findings, we present a simple model that summarizes our new insights into the formation and mobility of colloidal As in aquatic ecosystems. In this context, amorphous As_xS_y particles can present harmful effects to micro- and macro-biota not foreseen in bulk As material.

Introduction

Our research group identified for the first time the discharge of amorphous, colloidally suspended particles (20–400 nm) rich in As and S in hydrothermal fluids of a shallow marine system located near the coast of the Island of Milos (Greece) (Durán-Toro et al., 2019). However, the environmental parameters involved in the formation and stabilization of the material remained unclear. The shallow vents off Milos consist of hy-

* Corresponding authors.
E-mails: vicente.mdt@gmail.com (V. Durán-Toro), michael.maas@uni-bremen.de (M. Maas).

drothermal discharges of hot acidic fluids (up to 115 °C, pH 4–6) and gases (e.g. CO_2, H_2S), where dissolved arsenite (78 µmol/L) and sulfide (3 mmol/L) are released into the water column and are known to form larger yellow As_xS_y precipitates (> 400 nm), which rapidly sink to the sea floor (Bühring and Sievert, 2017; Godelitsas et al., 2015; Price et al., 2010; Price et al., 2013). So far, the toxic metalloid arsenic has been characterized in marine environments mainly as dissolved (i.e. arsenite and arsenate) and mineral species (Price et al., 2010). Therefore, better understanding of the geochemistry of colloidal arsenic particles in marine environments is needed, particularly to assess the toxicological implications of highly mobile suspended nanoparticles.

As is well-described for biominerals like calcium carbonate or calcium phosphate, further parameters besides temperature, pH or ratio between soluble species in the reaction could play a key role in As and S precipitation, particularly regarding the final morphology of the precipitates or the formation of a nanoparticulate phase. For example, biomineralization processes can be assisted by poly-acidic molecules, which can facilitate the stabilization of amorphous nanoparticles (Cai and Tang, 2008; Chiu et al., 2012; Fu et al., 2005). Another example of additive-controlled biomineralization is the formation of iron sulfide nanoparticles in magnetotactic bacteria, which depends on specific cysteine residues to trigger and stabilize the nanostructures inside the magnetosomes (Bazylinski et al., 1991). These examples indicate that organic molecules present in marine ecosystems as organic matter might also strongly influence metal and metalloid precipitation processes in hydrothermal vent systems (Langner et al., 2012).

These principles have also been applied for the synthetic preparation of nanoparticles. Here, organic additives are utilized to control particle nucleation, growth, colloidal stabilization and surface reactivity of nanomaterials (Durán-Toro et al., 2014; Khan and Talib, 2010; Lau and Hsu-Kim, 2008; Ubale et al., 2013). For example, the growth rate of zinc sulfide nanoparticles can be decreased in the presence of thiol containing additives (cysteine and glutathione, GSH), and the morphology of Ag nanoparticles can be tuned based on additive crosslinking reactions by increasing the concentration of the ligand cysteine, changing from quantum dots to nanorods configurations (Khan and Talib, 2010; Lau and Hsu-Kim, 2008). The surface reactivity of cadmium sulfide/telluride nanocrystals towards other metals like copper can be controlled by the capping agent GSH (Durán-Toro et al., 2014).

The precipitation of arsenic sulfide species has been previously studied based on the pH and temperature of the system (Eary, 1992; Godelitsas et al., 2015; Price et al., 2010; Rochette et al., 2000; Welch and Stollenwerk, 2003). If the pH or temperature decreases, the solubility of the sulfide species decreases as well, allowing the stabilization of a new solid phase (Eary, 1992). The precipitation of the arsenic and sulfur rich mineral orpiment has been demonstrated at room temperature and pH below 5, describing the formation of a precipitate when an excess of soluble sulfide in respect to arsenic (2:1) was present in solution (Rochette et al., 2000). However, the resulting material was not further characterized and the formation of nanoparticles was not addressed by the authors Rochette et al. (2000). On the other hand, organic matter has been hypothesized to interact with arsenic by phenolic OH groups, adducts formation with carboxylate groups stabilized by H bonds or hydrophobic interactions. Moreover, it has been shown that OM from peat samples (rich in sulfur atoms), can establish covalent bonds between S^{2-} and As^{3+}, playing an active role in arsenic immobilization and furthermore modifying the crystal phase of the analyzed precipitate (Langner et al., 2012). Likewise, the deposition of As_2S_3 thin films can be controlled by the presence of acidic additives as has been demonstrated for oxalic acid, changing the grain size from 31 to 11 nm and film thickness from 383 to 207 nm, without and with the additive (respectively) during chemical bath deposition experiments (Ubale et al., 2013). To the best of our knowledge no further deposition or precipitation experiments of As_2S_3 or any As_xS_y materials using thiol-containing additives have been published. Particularly the formation and stabilization of an amorphous nanoparticle phase have not been studied in detail.

In this context, we designed a study that experimentally recreates conditions of the described hydrothermal vent system off Milos in order to better understand the formation of the recently discovered colloidal As_xS_y phases. This will allow us to expand our knowledge on As geochemistry and consequently on how the toxicity of As is modified in marine ecosystems. To this end, we investigate the influence of parameters like concentrations, temperature and pH on the nucleation, growth and stability of As_xS_y. Furthermore, the presence of OM rich in thiol groups (-SH) and its influence in nucleation, growth, stability or crystal phase of the colloidal As material was evaluated. This we addressed by using cysteine and GSH as additives in the precipitation reaction. The resulting material was characterized by high resolution electronic microscopy, selected area electron diffraction, optical density measurements and dynamic light scattering.

1. Materials and methods

1.1. *Reagents and materials*

All reagents employed during experimental procedures, $NaAsO_2$, $NaS_2.9H_2O$, HCl (37%), L-cysteine hydrochloride, glycine hydrochloride and blue silica glass beads (desiccator agent) were purchased from Sigma Aldrich (Darmstadt, Germany) at analytical grade. Dilution of reagents was done in ultra-pure Milli-Q water (18.2 MΩ·cm). Anoxic experimental conditions were achieved by purging with N_2 gas from Linde (Dublin, Ireland). Reaction syntheses were carried out in polypropylene tubes acquired from Thermo Fisher Scientifc (Massachusetts, United States). Filtration was performed using polycarbonate Whatman® membranes with 0.2 µm pore size and 25 mm diameter size. Aluminum sample holders obtained from AMCO (Bremen, Germany) and formvar-coated copper-grids from Sigma Aldrich were used in electron microscopy analysis.

1.2. *Arsenic sulfide precipitation experiments*

The precipitation of arsenic was based on (Rochette et al., 2000) and adapted considering environmental hydrothermal

conditions . A 1 mol/L sodium arsenite ($NaAsO_2$) solution was prepared with Milli-Q water, aliquots of 1 mL were poured into Eppendorf tubes of 1.5 mL and stored at –20 °C. Sulfur containing additives (cysteine and glutathione, GSH) and glycine were prepared as 100 mmol/L stock solutions in water. A 1 mol/L Na_2S solution was prepared in a closed chamber at N_2 atmosphere. Afterwards, Na_2S was dissolved in autoclaved Milli-Q water previously cooled under N_2 flux to remove O_2 from solution. $Na_2S{\cdot}9H_2O$ stock solution was stored in sealed serum bottles at 4 °C. For the precipitation experiments, the reaction was carried out at different precursor ratios (S:As), pH and temperatures. The order of addition of the reagents remained the same in every experiment. Firstly, $Na_2S{\cdot}9H_2O$ was added to 35 mL of Milli-Q water, with final concentrations of 0, 0.6, 1.5, 2.1 or 3 mmol/L; secondly, additives were added to a final concentration of 1 mmol/L; thirdly, pH 3–4 was adjusted with 1 mol/L HCl; and finally after vigorous agitation, arsenite was added to a final concentration of 300 µmol/L. As soon as arsenic was added to the solution, the reaction mixtures were incubated at different temperatures (25, 45 and 75 °C) to simulate a temperature gradient present in natural systems. pH monitoring of the experiments was performed using a FiveEasy pH meter (Mettler-Toledo; Ohio, United States) and measurements were done every 20 min in the first hour, then the pH was measured once per day during three days of incubation.

1.3. *UV–Vis spectrophotometry*

Samples from different arsenic sulfide precipitation experiments were collected for analyzing UV-Vis spectra between wavelengths of 300 and 550 nm at several time intervals. Spectra were obtained using a Spectrophotometer UV-1280 (Shimadzu) with a quartz cuvette. Samples were analyzed unfiltered to obtain the optical density as a result of both light scattering and absorption of the particles suspended in solution.

1.4. *Dynamic light scattering*

Samples from different arsenic sulfide precipitation experiments were collected for analyzing particle size distribution by dynamic light scattering (DLS). Particle size distributions were obtained using a Zetasizer ZSP (Malvern) with the refractive index of As_2S_3 (2.65) as reference material (Rodney et al., 1958). Samples were analyzed unfiltered to obtain a representative scattering effect of all particles suspended in solution.

1.5. *Scanning electron microscopy coupled to energy-dispersive X-ray spectroscopy (SEM-EDX)*

Morphology, size and elemental composition of particulate material (> 200 nm) was studied by SEM-EDX analysis. Here, 200 nm pore-size polycarbonate membranes were used to collect arsenic sulfide precipitates at different reaction times and temperatures as described before (Durán-Toro et al., 2019). For SEM sample preparation, particles collected on the filters were dried in a desiccator using silica glass beads (5 days). For each filtration, 5 mL of sample was used to assure proper particle abundance on the filter. An iSUPRA 40 SEM (Zeiss) with an EDX detector (Bruker, XFlash 6|30) was operated at low voltage (3–5 kV) for high definition images and at 15 kV for EDX spectrum determination. EDX spectra were performed on each sample, accounting for at least 5 spots of a 5 μm^2 area of analysis.

1.6. *Transmission electron microscopy coupled to selected area electron diffraction (TEM-SAED)*

Morphology and crystal phase identification of the synthesized particles was studied by TEM-SAED analysis of particles formed during arsenic sulfide precipitation experiments at different temperatures of reaction or in the presence of additives. For TEM sample preparation, 5 µL of diluted (1:100) particle suspension were deposited on a carbon-coated copper grid and dried in a desiccator overnight. A FEI Titan microscope with SAED was operated at 80 to 300 kV depending on electron beam sensitivity of the particles.

2. Results

2.1. *Initial particle characterization*

Arsenic and sulfur precipitation experiments were adapted from a simple protocol based on the reaction of sodium arsenite ($NaAsO_2$) with sodium sulfide (Na_2S) in order to study the formation of a particulate fraction mimicking environmental hydrothermal conditions, which are characterized by acidic pH, elevated temperatures and high content of dissolved arsenic and sulfuric species (Durán-Toro et al., 2019; Rochette et al., 2000). In the reaction, the initial pH was adjusted to 3–4 prior to the addition of arsenite without presence of a buffer solution to avoid interaction of an arsenic sulfide phase with buffer molecules or ions. The pH was monitored during the experiments and showed no variations during the reaction (Appendix A Fig. S1). Fig. 1a shows an SEM micrograph of the precipitated colloidal particles collected on 200 nm polycarbonate filters. The particles exhibited spherical shapes and diameters around 200 nm. EDX analysis (Fig. 1b) shows that the particles are rich in As and S. A peak of oxygen (O) in the EDX spectrum suggests the presence of oxidized forms of either As or S. The strong peak of carbon (C) stems from the polycarbonate filter substrate. The normalized atomic weight percentage (S:As [Atom. %]) of the particles indicate a ratio close to 6, which differs from arsenic sulfide minerals like orpiment or amorphous arsenic sulfide (As_2S_3) with a theoretical number of 1.5 or realgar (As_4S_4) with a value of 1.

The presence of colloidal particles is evidenced by changes in turbidity of the reaction medium as a result of light scattering in the UV-vis wavelength range (Tyndall effect). Consequently, optical density (OD) spectra of the unfiltered reaction solutions were obtained in the wavelength range of 300–550 nm. Fig. 2 shows the OD spectra of different reaction solutions with As and S precursors at initial ratios (S:As) from 2:1 to 7:1. The spectra show a colloidal light scattering pattern with an increase of Rayleigh scattering in an exponential manner at small wavelengths (300–400 nm, Fig. 2). No variations over time (0 to 24 hr) suggest that the reaction finished at the beginning of the observed time period and that the particles remained suspended at 25 °C and pH close to 4 during the first 24 hr (Appendix A Fig. S2). The size distribution of the

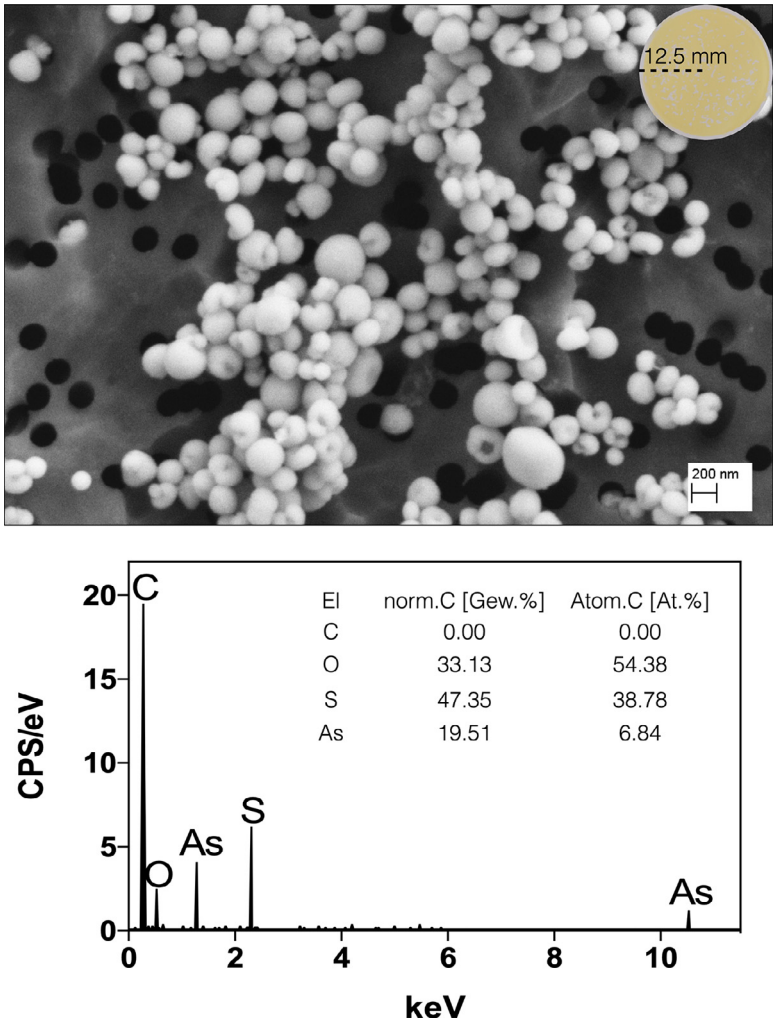

Fig. 1 – SEM-EDX analysis of the particulate fraction formed during As and S precipitation. The SEM image (a) shows the presence of spherical particles with diameters around 200 nm. The upper right inset shows a photograph of the yellow precipitate obtained after filtration. The EDX spectrum (b) of colloidal particles shows main peaks for As and S. Table legend: El., element; norm. C [wt.%], weight percentage normalized by C abundance; atom. C [at.%], atomic percentage normalized by C abundance. (For interpretation of the references to color in this figure legend, the reader is referred to the web version of this article.).

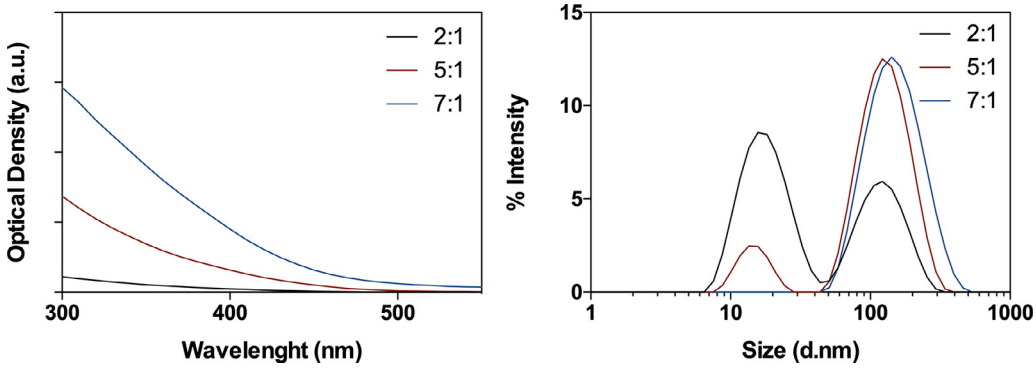

Fig. 2 – Absorbance spectra and DLS analyses of reaction solutions for As and S precipitation after 24 h of incubation at 25 °C and pH 3 - 4. Optical density spectra (left) and DLS (right) of the reaction medium with different S and As precursors ratio (2:1, 5:1, 7:1; PDI: 0.55, 0.48 and 0.21, respectively).

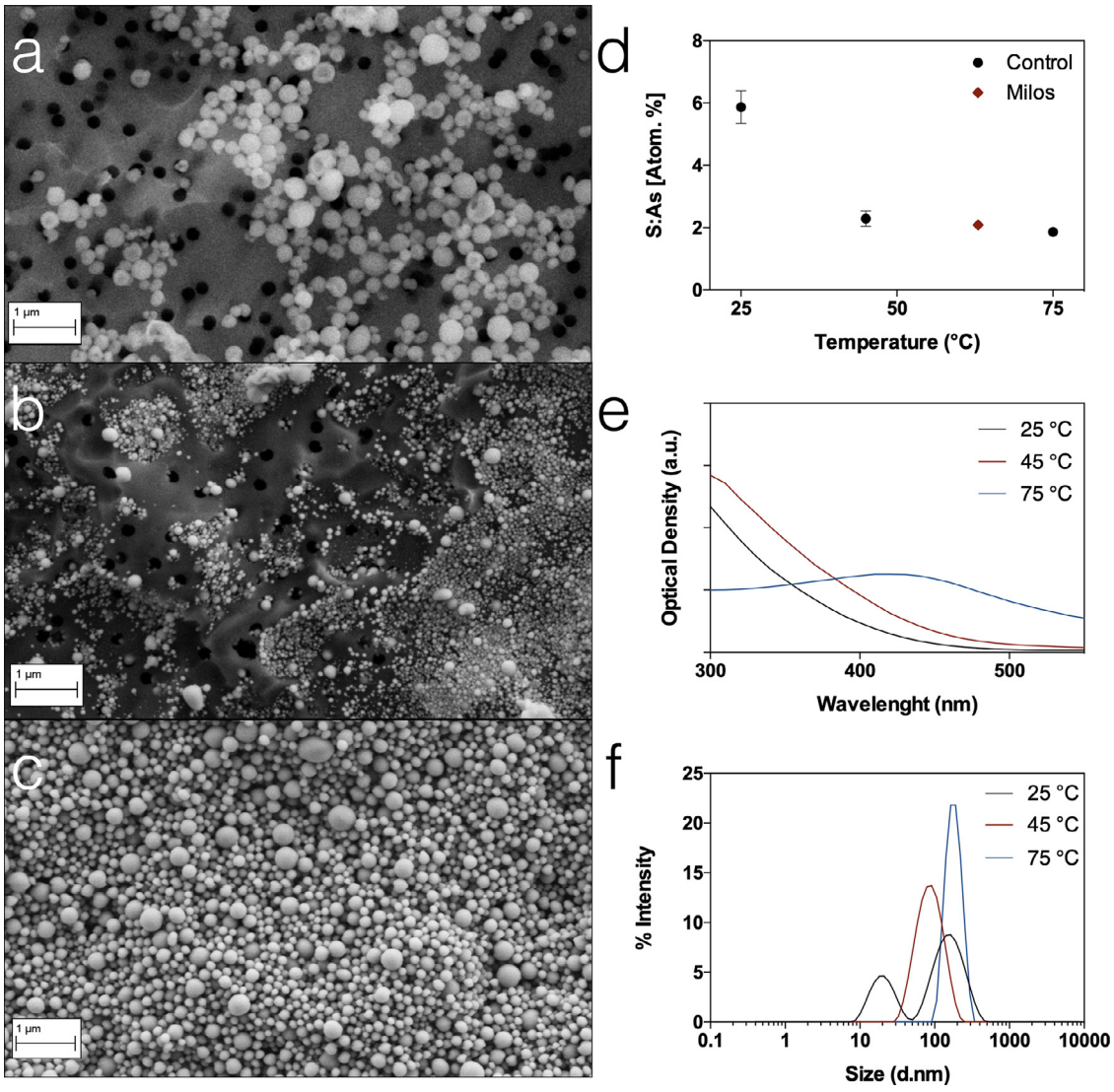

Fig. 3 – Influence of temperature on colloidal particle formation during As and S precipitation. (a), (b), and (c) SEM images of colloidal particles collected by filtration of reaction medium at temperatures 25, 45 and 75 °C, respectively, on polycarbonate 0.2 µm membranes. Aliquots were taken for filtration after 24 h with initial ratio of S:As precursors of 5:1. (d) shows the S:As ratio in the samples obtained from EDX analysis. The standard deviation of each sample was calculated from at least five independent measurements. The red rhombus symbol represents the Atom% of As-S-rich nanoparticles described in Milos (Durán-Toro et al., 2019). (e) Optical density spectra (300–550 nm) of unfiltered samples (containing the colloidal particles) from reaction synthesis at different temperatures. (f) DLS analysis of unfiltered samples from reaction synthesis at different temperatures.

unfiltered synthesized particles in suspension was evaluated by dynamic light scattering (DLS) (Fig. 2), showing a bimodal distribution in the intensity-weighted size distribution with major particle sizes at 13 and 140 nm and a moderately high polydispersity index (PDI > 0.2, Fig. 2) when low precursor ratios were applied (2:1 and 5:1). However, when a higher ratio (7:1) was established, the smaller particle sizes disappeared, presenting mostly particles with a size close to 140-160 nm and a narrower size distribution with PDI < 0.2.

2.2. *Temperature-dependent particle synthesis*

The influence of temperature (25–75 °C) was studied at a fixed S:As ratio of 5:1, which mimics soluble sulfide and As concentrations as well as temperatures present at hydrothermal systems (Durán-Toro et al., 2019; Price et al., 2010). Fig. 3a, b and c, show the particulate fraction collected on 200 nm polycarbonate filters after 24 h at 25, 45 and 75 °C, respectively. Spherical particles with a size ranging from 20 to 300 nm could be observed in the analyzed filtrates (Fig. 3 a–c). The density of the particle coverage on the filters suggested a correlation between reaction temperature and yield (Appendix A Table S1, Fig. S3 and Fig. 3). The decrease in S:As [Atom. %] as determined by EDX correlated to increasing temperatures and exhibited similar values to amorphous arsenic sulfur nanoparticles detected in the hydrothermal system off Milos (Fig. 3d) (Durán-Toro et al., 2019). Fig. 3e shows the changes in the OD

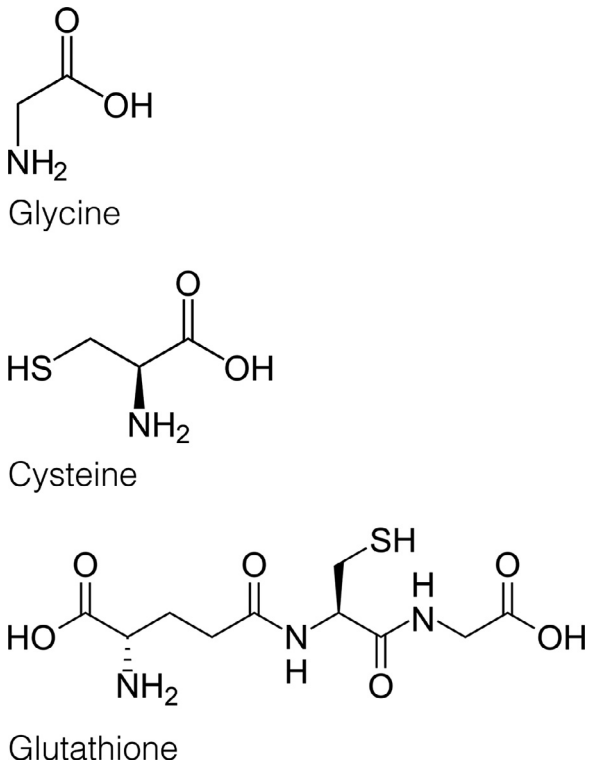

Fig. 4 – Chemical structure of additives used during As and S precipitation experiments.

spectra of the reaction medium at different incubation temperatures. At 45 °C, an increase in the optical density was observed compared to 25 °C (Fig. 3e). However, at 75 °C, the spectrum is no longer dominated by Rayleigh scattering but shows a broadband optical density with a shallow maximum at 450 nm (Fig. 3e). This is most likely an effect of the dominating larger particles which cause wave-length-independent Mie-scattering (Fig. 3d). The size distribution determined by DLS was also influenced by the reaction temperature, showing larger particles for incubations at higher temperatures (Fig. 3f) and PDI values of 0.62, 0.12 and 0.045 for reaction temperature of 25, 45 and 75 °C, respectively. The temperature effect resembles the variations in size distribution observed in changes of precursors ratio, where the smaller particles disappeared and only bigger particles with a peak diameter size close to 140–160 nm remained in solution (Fig. 3f).

2.3. *Particle synthesis in the presence of thiolic additives*

In order to evaluate the possible role of thiols in the formation and stabilization of the colloidal As and S rich particles under environmental hydrothermal conditions, the morphology, elemental composition and particle size distribution of the formed colloids were studied in the presence of thiolic additives. The thiols cysteine and GSH were chosen as reaction additives as examples for thiol-containing organic matter. Since the chemical structures of these thiols contain other functional groups, especially COOH and NH_2 (Fig. 4), glycine was used as an additional control to evaluate the effects of non-thiolic groups on the formed As-S phase.

Fig. 5a–d show the morphology and size of the particles collected on polycarbonate filters from the reaction medium at 25 °C after 24 h of incubation with and without additives. Fig. 5a and b show nanospheres with particle diameters close to 200 nm obtained from synthesis without (Fig. 5a) and with glycine (Fig. 5b). Remarkably, when cysteine or GSH were added, agglomerated ultra-small particles were formed (Fig. 5c and 5d, respectively). EDX analysis indicated As and S as the main constituents (data not shown), for conditions both with and without additives. The S:As [Atom.%] ratio in the different samples suggests a change in chemical composition of the material in the presence of thiolic additives (Fig. 5e). In the presence of cysteine and GSH, the S:As [Atom.%] values decrease compared to no additive or glycine (Fig. 5e). Size distribution analysis by DLS (Fig. 5f) substantiate these observations, showing two major particles sizes for the control and glycine treatments as before and a large increase in particle size in the presence of a thiol containing additive. When cysteine is used in the reaction, particles exhibited a broad size distribution with a single peak from 20 to 200 nm. When GSH was added, a significant increase to >1 μm was observed (Fig. 5f). One explanation for these broad size distributions might be the agglomeration of the smaller particle phase which is also present in the control samples. These ultra-small particles possibly escape the filter without additives, but might lose their colloidal stability as a result of their interaction with the thiolic additives resulting in agglomerates which are collected by the filter. Furthermore, the smaller particle phase might be a precursor from which the larger particles form, and this transformation could be inhibited by the additives.

Fig. 6a–d shows the morphology and size of particles formed at 75 °C, with and without additives and after 24 h of incubation. The micrographs in Fig. 6a (no additive) and b (glycine) show spheres with very similar particle diameters (100 to 300 nm). When thiols were added to the synthesis, smaller and agglomerated particles were observed. Instead of the ultra-small particles observed at lower temperatures with cysteine and GSH, ovoid particles were found, with a size ranging from 20 to 300 nm (Fig. 6c and d). Interestingly, analyses of the S:As [Atom.%] ratio in the samples suggests that the chemical composition is controlled by temperature rather than by the thiols (Fig. 6e). The S:As [Atom.%] ratio of the material remained similar when compared to the control without additive or in the presence of glycine, reaching values between 1.9 and 2.3 (Fig. 6e). The size distribution analysis (Fig. 6f) correlates to the observations from the SEM images, showing in the control and glycine samples a major particle size of 180–200 nm and a broader range of particle diameters in the presence of thiols. When cysteine and GSH were used in the reaction, particles exhibited diameters between 30 and 200 nm (Fig. 6f).

Optical density (OD) spectra of the reaction synthesis at 25 or 75 °C with different additives were studied over time (24 and 72 h) (Fig. 7). No major differences were observed when glycine was used as an additive at any given condition (Fig. 7). In the presence of cysteine or GSH, an increase in the OD was observed after the first 24 h of incubation (25 °C) when compared to the control and glycine addition (Fig. 7). Once the temperature of incubation was increased to 75 °C, the OD spectra of the control, glycine and GSH showed broad-band ad-

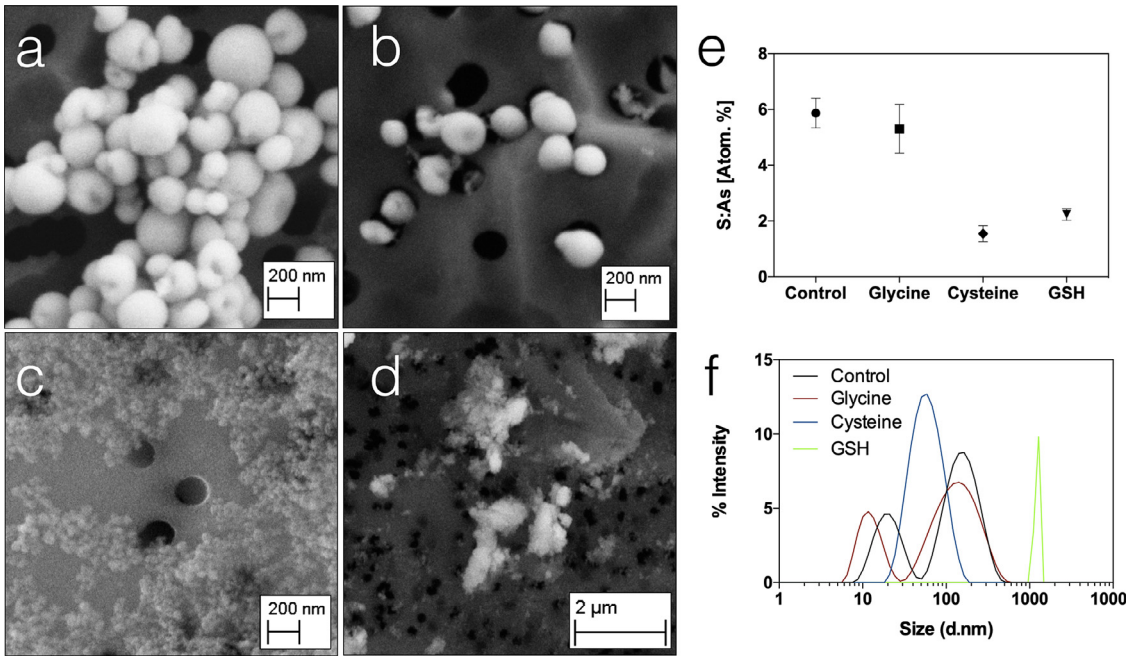

Fig. 5 – SEM-EDX and DLS analyses of colloidal particles synthesized in the presence of thiol additives at 25 °C. SEM images of the colloidal particles collected on polycarbonate filters (0.2 µm pore size) after 24 h incubation at 25 °C (a) without additive (b) with glycine, (c) cysteine and (d) GSH. (e) EDX analysis of S:As [Atom. %]. Standard deviations correspond to at least 3 measurements per sample. (f) DLS of particles size distribution in unfiltered reaction medium.

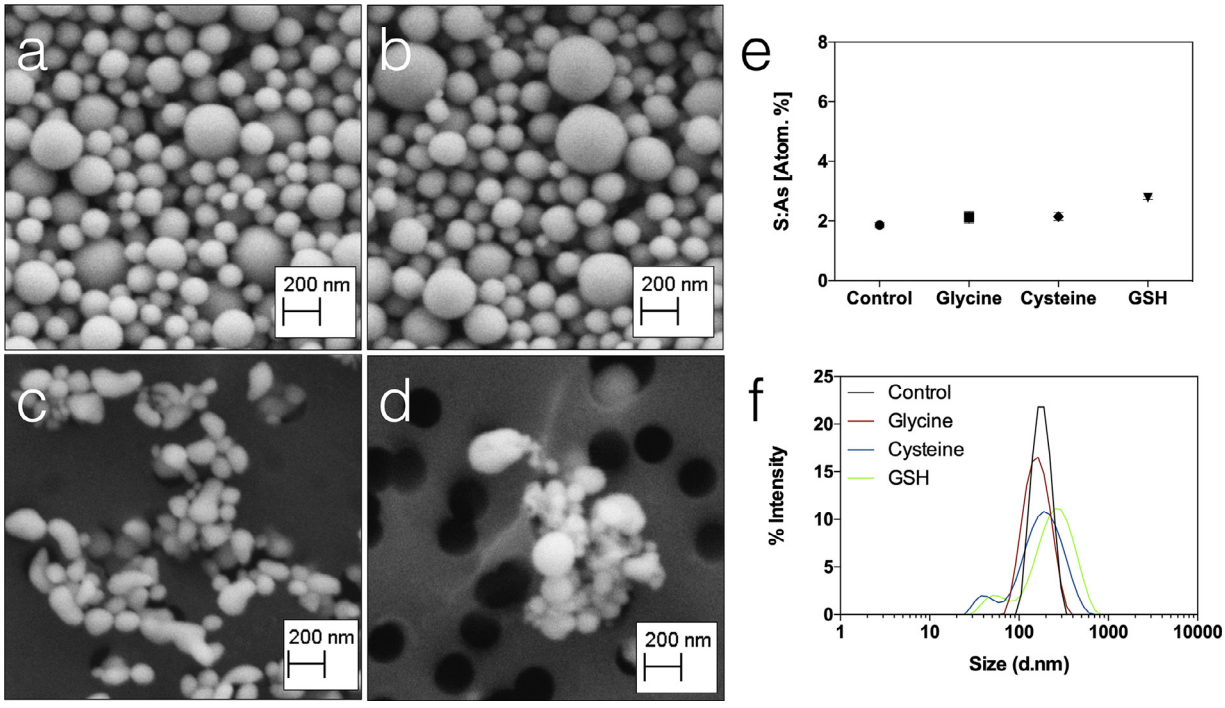

Fig. 6 – SEM-EDX and DLS analysis of colloidal particles synthesized in the presence of thiolic additives at 75 °C. SEM images of the colloidal particles collected on polycarbonate filters (0.2 µm pore size) after 24 h incubation at 75 °C (a) without additive, (b) with glycine, (c) cysteine and (d) GSH. (e) EDX analysis of S:As [Atom. %]. Standard deviations correspond to at least 3 measurements per sample. (f) DLS of particle size distribution in the unfiltered reaction medium.

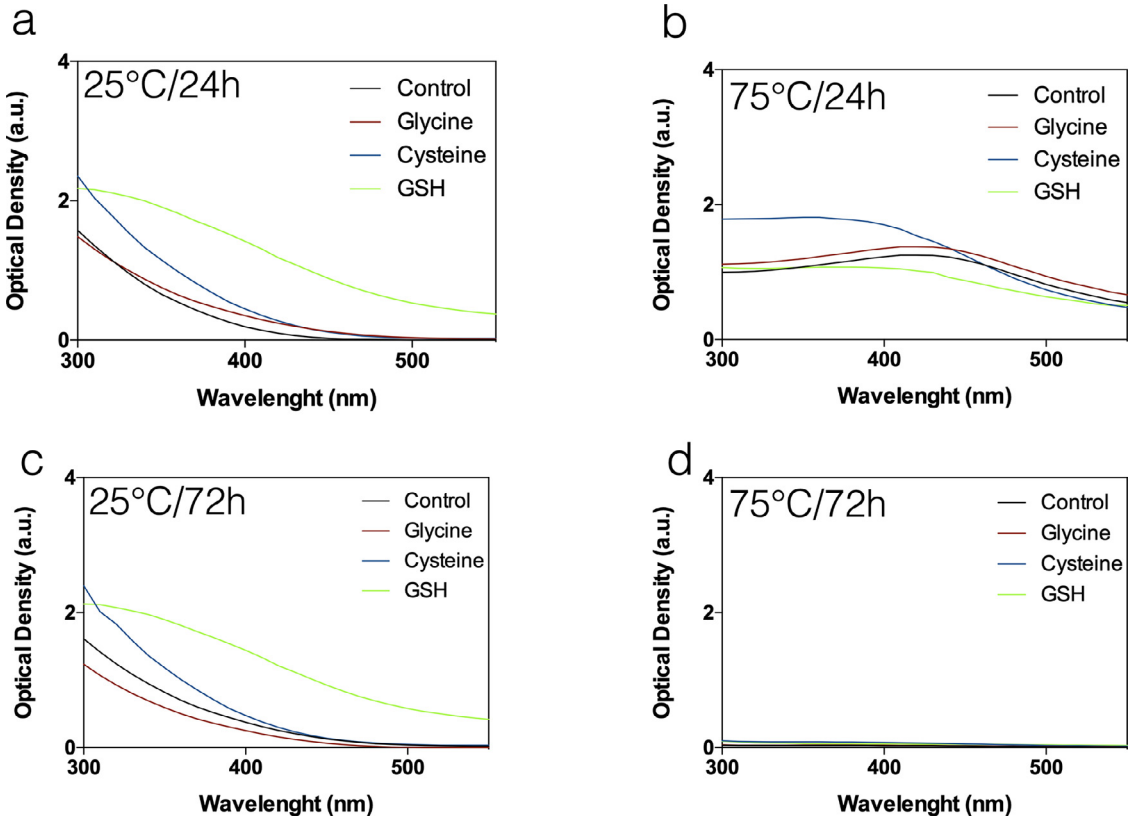

Fig. 7 – OD spectra of the unfiltered reaction medium at different temperatures, incubation times and with thiolic additives at S:As [Atom. %] 5:1. As and S precipitation experiments were carried at: (a), 25 °C incubation during 24 hr; (b), 75°C incubation during 24 hr; (c), 25°C incubation during 72 hr and (d), 75 °C incubation during 72 hr.

sorption with a shallow maximum between 400 and 500 nm (Fig. 7b). However, when cysteine was added to the reaction, a mixture of Rayleigh and Mie scattering was observed, with a maximum at 420 nm (Fig. 7b) and an increase at lower wavelengths. After 72 h of incubation, no further modification was noticeable in the spectra with or without additives at 25 °C (Fig. 7c). Nonetheless, the OD signal associated with the particles vanished completely after 72 h at 75 °C with or without additives (Fig. 7d, right). This result indicates the dissolution of the arsenic sulfide phase after 72 h, which was corroborated by the absence of As- and S-rich colloidal particles in the SEM-EDX analysis of the samples on polycarbonate filters (data not shown).

2.4. *Crystal phase analysis*

Crystal phase identification was carried out by TEM-SAED experiments of particles formed in reaction solutions at different temperatures (25 and 75 °C) and in the absence (control) and presence of thiolic additives (cysteine and GSH). The TEM images (Fig. 8) of drop-cast, unfiltered aliquots of the reaction medium confirmed the size and morphology of the particles as described before, showing a spherical morphology and sizes close to 100 nm for control conditions at 25 and 75 °C after 24 h of incubation (Fig. 8a and b). When cysteine was added to the reaction at 25 °C, the agglomerated ultra-small particles described earlier can be observed (Fig. 8c). When the temperature was elevated to 75 °C the ultra-small particles disappeared and instead ovoidal particles were found in smaller agglomerates (Fig. 8d). When GSH was used as additive, the formation of larger particles was detected at 25 °C (Fig. 8e), while at higher temperatures a similar ovoidal morphology could be identified (Fig. 8f). SAED analysis of the particles indicates that all particles types are amorphous, evidenced by the absence of crystalline long-range order in all of the formed particles, independent of temperature or the presence of additives during precipitation (Fig. 8).

3. Discussion

3.1. *Proposed mineralization mechanism at the hydrothermal vent system off Milos*

Understanding the mineralization of arsenic sulfide represents a key step in elucidating the geochemistry of As in different ecosystems (Godelitsas et al., 2015; Langner et al., 2012). In recent years, novel mechanisms of biomineralization (e.g. for $Ca_5[OH(PO_4)_3]$ or $CaCO_3$), have highlighted the relevance of nanoparticles in these processes and how environmental parameters like temperature and organic matter (organic molecules) contribute in the stabilization of the nanostructures (Bazylinski et al., 1991; Cai and Tang, 2008; Chiu et al., 2012; Fu et al., 2005). Current models of As and S precipi-

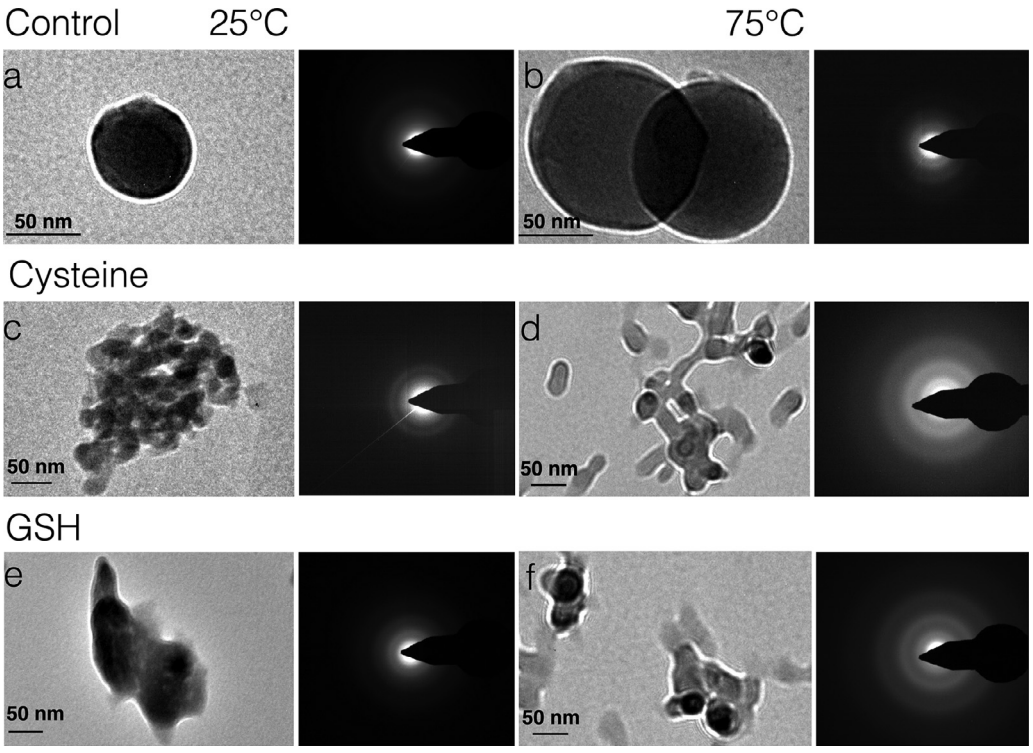

Fig. 8 – TEM-SAED analysis of colloidal particles synthesized in the presence of thiol additives at different temperatures. TEM images (left) and corresponding SAED diffractogram (right) of the colloidal particles after 24 h incubation without additives at 25°C (a), at 75°C (b) and incubated with cysteine at 25 °C (c), at 75 °C (d) or in the presence of GSH at 25 °C (e) and at 75 °C (f). SAED analysis shows the absence of crystalline long-range order at every condition.

tation under environmental conditions have not yet considered colloidal As particles (20 400 nm) as part of the process (Bissen and Frimmel, 2003; Durán-Toro et al., 2019; Eary, 1992; Godelitsas et al., 2015; Rochette et al., 2000). Nonetheless, our results (Fig. 1), support the idea of colloidal As particle formation as a natural phenomenon occurring during As and S precipitation in the environment when an excess of soluble sulfide relative to As occurs (S:As of 2:1, Fig. 1). Most of the reaction conditions for As and S precipitation in the present work resemble shallow water hydrothermal systems (pH 4 – 6; 30–90 °C; As: 78 µmol/L; S^{2-}, HS^{-}: 3 mmol/L), and constitute a first approach for understanding the influence of temperature on the formation of As colloidal particles (Godelitsas et al., 2015; Price et al., 2013). Only dissolution assays of arsenic sulfide minerals have been reported in the literature so far, indicating a decrease in their stability with increasing temperature and amorphous phases of arsenic sulfide minerals as the main precipitate at temperatures near 90 °C (Eary, 1992). Based on the influence of temperature, the discovery of amorphous As and S rich nanoparticles in the shallow hydrothermal system off Milos was explained as a consequence of a temperature drop due to mixing of seawater and hot (> 60 °C) hydrothermal fluids (Durán-Toro et al., 2019). Mixing of As and S rich fluids and seawater was attributed to cause an oversaturation of the arsenic sulfide species due to their low solubility at temperatures of 20 to 25 °C (Durán-Toro et al., 2019). Nonetheless, the data presented here indicate a more complex explanation (Fig. 3). In an initial step, during the first 24 h of reaction, the elevated temperature exhibited an enhancing effect on particle nucleation, boosting the yield of nanoparticles (Fig. 3a–c). This relation between temperature and reaction synthesis was further evidenced by the different S and As content in the particles formed at 45 or 75 °C, which was remarkably similar to those found in the natural nanoparticles discovered in the Milos hydrothermal system (Fig. 3d). Furthermore, a total dissolution of the particles after 72 h of incubation at 75 °C (Fig. 7d) was detected. Conversely, at 25 °C, the integrity of the signal associated with the presence of the colloidal material remained unaltered (Fig. 7c). The analyzed temperatures (up to 75 °C) are similar to values recorded in shallow hydrothermal systems which therefore suggests that dissolution of initially formed particles may also occur within 24 h in a natural hydrothermal system. However, it is likely that particles formed under high temperature hydrothermal conditions remain stable once the fluids are mixed with colder seawater. This suggests that As and S rich particles with similar S:As [Atom. %] ratio to the herein described colloidal particles are stabilized in pore-water (seawater in the sediments) and hydrothermal fluid samples from Paleochori bay, avoiding dissolution by high temperatures once mixed with seawater (Fig. 9) (Durán-Toro et al., 2019).

The mineralization mechanism could potentially be complicated by the oxidation of the As ions. However, the oxidation rate of dissolved As^{+3} in water and in the presence of air is slow. Only 25% of As^{+3} is oxidized within 5 days when purging a solution initially containing 200 µg/L As^{+3} with air

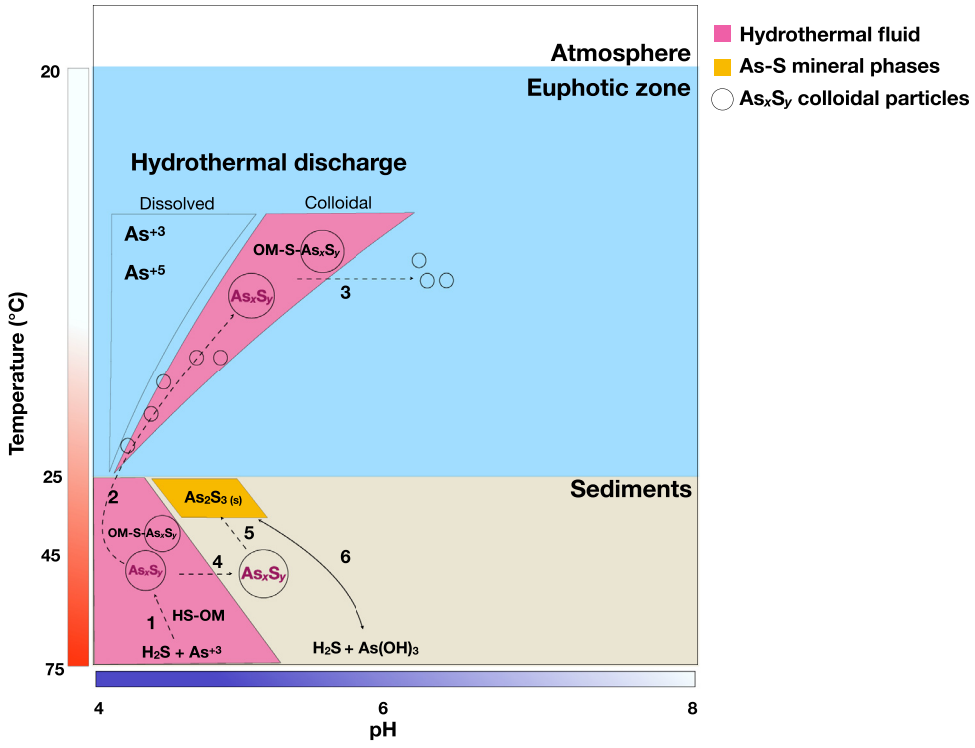

Fig. 9 – Geochemistry of As_xS_y colloidal particles in a shallow hydrothermal vent off Milos. Hydrothermal discharge, consisting of hot fluids (pink) rich in soluble sulfide (H_2S) and reduced forms of Arsenic (As^{3+}), emerges from the center of the vent generating a gradient of temperature and pH along the water column and sediments. (1) Sulfur and Arsenic species within the fluids and with or without the presence of organic matter rich in thiol groups (OM-SH) form stable amorphous colloidal particles. (2) the As_xS_y colloidal particles are transported through the sediments and into the water column as part of the colloidal fraction of the hydrothermal discharge. (3) As_xS_y colloidal particles are dispersed along the water column, contributing to the total amount of arsenic present in seawater. (4) As_xS_y colloidal particles diffuse along the sediments. (5) As_xS_y colloidal particles contribute to the formation of As and S rich mineral phases on the seafloor (yellow). (6) Precipitation of As and S rich mineral phases on the seafloor by direct interaction of a soluble precursor. Dashed arrows correspond to hypothetical reactions or transport processes of colloidal particles. (For interpretation of the references to color in this figure legend, the reader is referred to the web version of this article.)

(Clifford et al., 1983). 8% of As^{+3} can be oxidized within 60 min in solutions purged with pure oxygen (Frank and Clifford, 1986). Groundwater containing As^{+3} purged with air and pure oxygen showed that between 54% and 57% of As^{3+} were oxidized within 5 days (Kim and Nriagu, 2000). Our experimental designed showed the formation of colloidal particles in the first 1 hr of incubation and the scattering signal of the suspended particles to remain stable within the first 24 hr of incubation (Appendix A Fig. S2). Therefore, the low oxidation rate of the As^{+3} precursor (AsO_3^{3+}) within the first 24 hr by the oxygen present in the air strongly suggests the absence of As^{+5} during the formation of the colloidal particles.

3.2. *Influence of OM on the proposed mineralization mechanism*

The interaction between OM and metals in hydrothermal systems, specifically in shallow vents, has been previously shown to be a selective process in which co-precipitation or interaction of OM and elements like Fe or Cu dictates geochemical cycles in marine environments (Gomez-Saez et al., 2015; Kleint et al., 2015). Fig. 5 shows how the presence of thiol-containing additives during the precipitation of As and S altered the morphology, chemical composition and size distribution of the formed particles. At 25 °C and with the addition of cysteine, granular structures with an S:As [Atom. %] ratio lower than the control and a broader particle size distribution were observed (Fig. 5c, e and f). Similarly, with GSH, agglomerated ultra-small particles with a low S:As [Atom. %] ratio were detected (Fig. 5d, e and f). These findings drastically differ from the colloidal particles formed without thiolic additives (Fig. 5). The high affinity of As^{3+} species like arsenite for sulfhydryl (-SH) groups, suggests the stabilization of different As_xS_y phases based on the presence of thiol-containing additives. These novel As-S phases could be formed through a direct bond between the As and the S atom as suggested in the literature (Langner et al., 2012). These interactions of the additives with the nucleating particle phase might explain the changes in morphology and chemical composition (Figs. 5 and 6). The appearance of granular agglomerates correlates with the previous description of As_2S_3 films formed due to the interaction with additives (Ubale et al., 2013). These re-

sults suggest an analogous phenomenon occurring in the hydrothermal system off Milos, where a similar range of morphologies, size, S:As [Atom. %] ratio and crystal phase was described (Durán-Toro et al., 2019). Thus, we suggest that thiols might have a strong impact upon nucleation and growth of As-rich colloidal material at low temperatures and in consequence on the mobility of the metalloid in marine environments, where OM rich in S represent a key component. Furthermore, our experiments suggest that the above-described effect of elevated temperatures dominates over the effect of the additives (Figs. 6 and 7). This can be particularly noted in the absence of agglomerated ultra-small particles even in the presence of additives at 75 °C. Instead, larger particles similar in morphology and composition to those formed at 75 °C without additives are generated. Most amino acids and short peptides do not undergo decomposition at temperature near 75 °C, and in the case of cysteine an oxidation to cystine and only a posterior degradation can be observed in minor quantities at temperatures close to autoclaving (100 °C) (Evans and Butts, 1949; Haberstroh and Karl, 1989; Weiss et al., 2018). However, decomposition of additives cannot be completely ruled out.

4. Conclusions

The synthesis of colloidal As particles was performed via the precipitation of water-soluble precursors at conditions mimicking those found at natural hydrothermal systems. The resulting colloidal particles exhibited a spherical shape, were rich in As and S, with a size range of 10 to 300 nm. Particle properties like size, polydispersity, yield or S and As atomic weight % ratio could be easily tuned by the synthesis parameters, particularly S and As precursor ratio or temperature. Additives like thiols furthermore represent a key parameter for colloidal particle formation at low temperatures, favoring the generation of As- and S-rich aggregates instead of individual and well-defined particles. However, the effects of higher temperatures dominate the process even in the presence of additives. Our findings are in agreement with previous reports of environmental and synthetic formation of As_xS_y species and suggests the precipitation of arsenic sulfide minerals through formation of arsenic-sulfur-rich colloidal particles in the presence of organic matter as a common step occurring in hydrothermal and other marine systems. Consequently, our findings can be potentially transferred to the hydrothermal vent system: During the initial exhaust of hot ($T > 60°C$) hydrothermal fluid particle formation takes place with high yield. The morphology, size and more importantly the S:As [Atom. %] ratio in the particles correlate with the particles generated at elevated temperatures and indeed exhibit values notably similar to As- and S-rich particles found in the shallow hydrothermal system off Milos (Greece). If the particles remained in this hot area, they would, however, dissolve again over time. Most likely, the particles are rapidly mixed with colder regions of sea water, where they remain mostly unchanged and colloidally suspended. The colloidal suspension of the amorphous particles then leads to extended mobilization of the colloidal phase, resulting in far-field dispersion of As in seawater. Consequently, our results suggest the precipitation of As and S rich colloidal particles as a natural phenomenon in environments with low pH within a temperature gradient and soluble sulfide exceeding As concentrations. This shows that an improved understanding of the formation, mobility and fate of As in marine environments in its colloidal phase is critical, and detailed comprehension of the harmful and chemical impact of arsenic-bearing nanomaterials might lead to novel regulations of pollutants and new insights into geochemical models.

Acknowledgments

This study was supported by Conicyt through a fellowship to VDT (Programa de Capital Humano Avanzado, BECAS-Chile, CONICYT, 72160570 Res. Convenio 7359/2015) and by the Deutsche

Forschungsgemeinschaft (DFG, Germany) through the Emmy Noether Program (grant BU 2606/1-1 to SIB). We would like to thank Reshma Kadam for her support in the Advanced Ceramics laboratories and Petra Witte for performing SEM analyses.

REFERENCES

Bazylinski, D.A., Frankel, R.B., Garratt-Reed, A.J., Mann, S., 1991. Biomineralization of iron sulfides in magnetotactic bacteria from sulfidic environments. In: Frankel, R.B, Blakemore, R.P (Eds.), Iron Biominerals. Springer, US: Boston, MA, pp. 239–255.

Bissen, M., Frimmel, F.H., 2003. Arsenic — a review. Part I: occurrence, toxicity, speciation, Mobility. Acta Hydrochim. Hydrobiol. 31, 9–18.

Bühring, S., Sievert, S., 2017. The shallow submarine hot vent system off Milos (Greece) – a natural laboratory to study hydrothermal geomicrobiology. In: Kallmeyer, J. (Ed.), Life in Extreme Environments, Life at Vents and Seeps.

Cai, Y., Tang, R., 2008. Calcium phosphate nanoparticles in biomineralization and biomaterials. J. Mater. Chem. 18, 3775–3787.

Chiu, D., Zhou, W., Kitayaporn, S., Schwartz, D.T., Murali-Krishna, K., Kavanagh, T.J., et al., 2012. Biomineralization and size control of stable calcium phosphate core–protein shell nanoparticles: potential for vaccine applications. Bioconjug. Chem. 23, 610–617.

Clifford, D., Ceber, L., Chow, S., 1983. Arsenic (III)/Arsenic (V) separation by chloride-form ion-exchange resins. In: Proceedings of the XI AWWA WQTC.

Durán-Toro, V., Gran-Scheuch, A., Órdenes-Aenishanslins, N., Monrás, J.P., Saona, L.A., Venegas, F.A., et al., 2014. Quantum dot-based assay for Cu^{2+} quantification in bacterial cell culture. Anal. Biochem. 450, 30–36.

Durán-Toro, V.M., Price, R.E., Maas, M., Brombach, C.C., Pichler, T., Rezwan, K., et al., 2019. Amorphous arsenic sulfide nanoparticles in a shallow water hydrothermal system. Mar. Chem. 211, 25–36.

Eary, L.E., 1992. The solubility of amorphous As_2S_3 from 25 to 90°C. Geochim. Cosmochim. Acta 56, 2267–2280.

Evans, R.J., Butts, H.A., 1949. Inactivation of amino acids by autoclaving. Science 109, 569.

Frank, P., Clifford, D.A., 1986. Arsenic (III) Oxidation and Removal from Drinking Water. Water Engineering Research Laboratory, Office of Research and Development EPA 600-2-86-021.

Fu, G., Valiyaveettil, S., Wopenka, B., Morse, D.E., 2005. $CaCO_3$ biomineralization: acidic 8-kDa proteins isolated from

aragonitic abalone shell nacre can specifically modify calcite crystal morphology. Biomacromolecules 6, 1289–1298.
Godelitsas, A., Price, R.E., Pichler, T., Amend, J., Gamaletsos, P., Göttlicher, J., 2015. Amorphous As-sulfide precipitates from the shallow-water hydrothermal vents off Milos Island (Greece). Mar. Chem. 177, 687–696.
Gomez-Saez, G.V., Riedel, T., Niggemann, J., Pichler, T., Dittmar, T., Bühring, S.I., 2015. Interaction between iron and dissolved organic matter in a marine shallow hydrothermal system off Dominica Island (Lesser Antilles). Mar. Chem. 177, 677–686.
Haberstroh, P.R., Karl, D.M., 1989. Dissolved free amino acids in hydrothermal vent habitats of the Guaymas Basin. Geochim. Cosmochim. Acta 53, 2937–2945.
Khan, Z., Talib, A., 2010. Growth of different morphologies (quantum dots to nanorod) of Ag-nanoparticles: role of cysteine concentrations. Colloids Surf. B 76, 164–169.
Kim, M.J., Nriagu, J., 2000. Oxidation of arsenite in groundwater using ozone and oxygen. Sci. Total Environ. 247, 71–79.
Kleint, C., Kuzmanovski, S., Powell, Z., Bühring, S., Sander, S., Koschinsky, A., 2015. Organic Cu-complexation at the shallow marine hydrothermal vent fields off the coast of Milos (Greece), Dominica (Lesser Antilles) and the Bay of Plenty. Mar. Chem. 173, 244–252.
Langner, P., Mikutta, C., Kretzschmar, R., 2012. Arsenic sequestration by organic sulphur in peat. Nat. Geosci. 5, 66–73.
Lau, B.L.T., Hsu-Kim, H., 2008. Precipitation and growth of zinc sulfide nanoparticles in the presence of thiol-containing natural organic ligands. Environ. Sci. Technol. 42, 7236–7241.
Price, R., Planer-Friedrich, B., Savov, I., Pichler, T., 2010. Arsenic cycling, thioarsenates and orpiment precipitation at a shallow sea hydrothermal system. In: Proceedings of the Arsenic in Geosphere and Human Diseases, As 2010 - 3rd International Congress: Arsenic in the Environment, Milos Island, Greece, pp. 66–68.
Price, R.E., Savov, I., Planer-Friedrich, B., Bühring, S.I., Amend, J., Pichler, T., 2013. Processes influencing extreme As enrichment in shallow-sea hydrothermal fluids of Milos Island. Greece Chem. Geol. 348, 15–26.
Rochette, E.A., Bostick, B.C., Li, G., Fendorf, S., 2000. Kinetics of arsenate reduction by dissolved sulfide. Environ. Sci. Technol. 34, 4714–4720.
Rodney, W.S., Malitson, I.H., King, T.A., 1958. Refractive index of arsenic trisulfide. J. Opt. Soc. Am. 48, 633–636.
Ubale, A., Kantale, J.S., Choudhari, D.M., Mitkari, V.N., Nikam, M.S., Belkhedkar, M., 2013. Characterization of nanostructured As_2S_3 thin films synthesized at room temperature by chemical bath deposition method using various complexing agents. Thin Solid Films 542, 160–166.
Weiss, I.M., Muth, C., Drumm, R., Kirchner, H.O.K., 2018. Thermal decomposition of the amino acids glycine, cysteine, aspartic acid, asparagine, glutamic acid, glutamine, arginine and histidine. BMC Biophys. 11, 2.
Welch, A.H., Stollenwerk, K.G., 2003. Arsenic in Ground Water: Geochemistry and Occurrence. Springer Science & Business Media.